J. Fluid Mech. (1994), *vol.* 269, *pp.* 169–198

On the dynamics of gravity currents in a channel

By JOSEPH B. KLEMP, RICHARD ROTUNNO AND WILLIAM C. SKAMAROCK

National Center for Atmospheric Research, Boulder, CO 80307, USA

(Received 19 November 1992 and in revised form 23 August 1993)

We attempt to clarify the factors that regulate the propagation and structure of gravity currents through evaluation of idealized theoretical models along with two-dimensional numerical model simulations. In particular, we seek to reconcile research based on hydraulic theory for gravity currents evolving from a known initial state with analyses of gravity currents that are assumed to be at steady state, and to compare these approaches with both numerical simulations and laboratory experiments. The time-dependent shallow-water solution for a gravity current propagating in a channel of finite depth reveals that the flow must remain subcritical behind the leading edge of the current (in a framework relative to the head). This constraint requires that $h_f/d \leqslant 0.347$, where h_f is the height of the front and d is the channel depth. Thus, in the lock-exchange problem, inviscid solutions corresponding to $h_f/d = 0.5$ are unphysical, and the actual currents have depth ratios of less than one half near their leading edge and require dissipation or are not steady. We evaluate the relevance of Benjamin's (1968) well-known formula for the propagation of steady gravity currents and clarify discrepancies with other theoretical and observed results. From two-dimensional simulations with a frictionless lower surface, we find that Benjamin's idealized flow-force balance provides a good description of the gravity-current propagation. Including surface friction reduces the propagation speed because it produces dissipation within the cold pool. Although shallow-water theory overestimates the propagation speed of the leading edge of cold fluid in the 'dam-break' problem, this discrepancy appears to arise from the lack of mixing across the current interface rather than from deficiencies in Benjamin's front condition. If an opposing flow restricts the propagation of a gravity current away from its source, we show that the propagation of the current relative to the free stream may be faster than predicted by Benjamin's formula. However, in these situations the front propagation remains dependent upon the specific source conditions and cannot be generalized.

1. Introduction

Cold-air masses flowing along the ground play an important role in a variety of atmospheric processes and often bear striking similarity to gravity currents produced in the laboratory. In analysing the propagation of atmospheric gravity currents, researchers have made broad application of a formula, proposed by Benjamin (1968), that relates the speed of a steady-state gravity current to the depth and density difference of the intruding stream as well as the depth of the effective channel that bounds the flow. However, in applying this relation to geophysical gravity currents, numerous apparent discrepancies have arisen that have spawned a variety of explanations and modifications to the formula. Even in laboratory studies of gravity currents, there are ambiguities in applying and interpreting Benjamin's result. In the present study, we use idealized theoretical models along with numerical models to

investigate the propagation of gravity currents and to evaluate the validity of Benjamin's formula. Stimulated by atmospheric applications and recognizing the linear nature of many cold-air boundaries, we shall focus primarily on two-dimensional Boussinesq flow.

Research on gravity currents has generally approached the topic from one of two different perspectives. One direction of research has used hydraulic (shallow-water) theory to study the evolution of gravity currents from a state of rest, while the other has investigated the steady-state characteristics of a gravity current that has already been established. Because the realizability of possible steady-state structures may depend on the factors producing them, both theories are needed, and moreover the relation between the two must be clearly established. The problem of a dense fluid initially at rest, that then spreads under its own weight after a retaining barrier is removed, is an appropriate paradigm for many atmospheric gravity currents. We review the hydraulic theory relating to this so-called 'dam-break' problem in §2. A result of this theory that is particularly relevant to the present study is that steady-state solutions are possible in the vicinity of the leading edge (or nose) of the advancing dense fluid if a certain type of boundary (front) condition is applied at the nose. Independent of the hydraulic theory, researchers have taken the steady gravity current as an empirically given fact, and then determined the relations that must therefore hold. This approach has led to formulae that relate the gravity-current speed to its depth – essentially the 'front conditions' required to provide closure in the shallow-water solutions. Benjamin's (1968) well-known formula is of this class and is reviewed, along with others, in §2.

In order to integrate these two approaches, we investigate further the dam-break problem within a channel of finite depth in §3. We follow the general approach of Rottman & Simpson (1983) (with some important modifications) and use the two-layer shallow-water equations with Benjamin's (1968) formula to determine the propagation speed of the leading edge of the current. This initial-value approach is revealing as it clearly shows the constraints that regulate both the upstream- (into the reservoir) and downstream-propagating disturbances. In particular, we find that the upstream-propagating disturbances form a rarefaction wave for reservoir depths h_0 less than one half the channel depth d, but steepen into an abrupt front for $h_0/d > 0.5$, and that the downstream-moving front cannot exceed a depth of $h_f/d = 0.347$.

Comparisons with laboratory data show that the shallow-water solutions, with Benjamin's formula used as a front condition, give a very good qualitative picture of the flow evolution, and its dependence on the external parameters of the problem. However, the theory does overpredict the gravity-current speed. Without further information, it is not clear whether the shallow-water theory itself, Benjamin's front condition, or the absence of surface drag, is responsible for this discrepancy.

To help resolve this issue, we present two-dimensional simulations for a continuous fluid with and without surface drag in §4. Without surface drag, the simulations indicate that Benjamin's formula in fact provides a good approximation to the steady flow-force balance. Including the effects of interfacial mixing which are absent in the shallow-water equations, the two-dimensional simulations are in closer agreement with the laboratory data. However, surface drag is finally needed to produce close quantitative agreement between the model and data.

Under certain circumstances, gravity currents may propagate faster than predicted by Benjamin's condition. We address this behaviour in §5 and conclude that it may occur when the front is constrained from propagating away from the source region. An overall summary of results and concluding remarks are given in §6.

2. Historical perspective

2.1. *Initial-value hydraulic solutions*

Much of the early interest in gravity currents arose in hydraulics research on topics such as intrusions of fresh or salt water in the vicinity of locks and estuaries, spreading oil spills, and collapsing dams. In these problems, the initial state is often well defined and research has focused on the evolution of the flow as two fluids of differing density come into contact. In summarizing research in this area, we focus on the basic question of how a relatively heavy fluid spreads relative to its environment, with emphasis on situations relevant to atmospheric flows.

The simplest theory for a spreading cold pool represents the cold fluid as a rectangle that conserves its area as its aspect ratio increases with time. This approach was explored by engineers concerned with oil spills (Hoult 1972), and predicts that at large time t the front speed decreases as $t^{-\frac{1}{3}}$, while the height decreases as $t^{-\frac{2}{3}}$. However, these results stand in contrast to observations of storm outflows and fronts that frequently exhibit fairly constant height and steady speed. This suggests that atmospheric gravity currents are often continually supplied with cold air.

A continuous supply of denser fluid is provided when an initially stationary semi-infinite reservoir of height h_0 spreads under its own weight, as illustrated in figure 1 (*a*). Although many of the early hydraulic studies focused on water–air systems in which the density difference is large, the same dynamical equations can be derived for fluids exhibiting smaller density differences using a suitably reduced value for the gravitational acceleration (cf. Stoker 1957, p. 388). Because of our interest in Boussinesq systems, we shall summarize these earlier studies based on the shallow-water equations including this reduced gravity, which for atmospheric flow can be expressed as

$$\frac{\partial u}{\partial t}+u\frac{\partial u}{\partial x}+g'\frac{\partial h}{\partial x}=0, \tag{1}$$

$$\frac{\partial h}{\partial t}+\frac{\partial uh}{\partial x}=0, \tag{2}$$

where h and u are the depth and horizontal velocity of the cold air (having potential temperature θ_0) spreading into an environment having potential temperature θ_1, and

$$g'=g\frac{\theta_1-\theta_0}{\theta_1}$$

is the reduced gravity.

In hydraulics, this is the well known dam-break problem, and was solved using the method of characteristics in terms of the characteristic variables $u\pm 2(g'h)^{\frac{1}{2}}$ propagating at speeds $u\pm(g'h)^{\frac{1}{2}}$, respectively. Saint-Venant solved this problem in 1843 assuming the height of the cold pool drops continuously to zero approaching the leading edge (see Keulegan 1950, or Stoker 1957). Following the downstream-propagating characteristic from far upstream in the reservoir where $u=0$,

$$u+2(g'h)^{\frac{1}{2}}=2(g'h_0)^{\frac{1}{2}}\equiv 2c_0, \tag{3}$$

and thus the leading edge moves downstream at speed $u_f=2c_0$. The leading edge of the depression wave moves upstream at speed $-c_0$ and the surface between these extremes maintains a parabolic shape as shown in figure 1 (*a*). At the original dam location, the flow remains just critical (i.e. the flow speed just equals the wave speed). Using $u_d=(g'h_d)^{\frac{1}{2}}$ together with (3) revealed that remarkably,

$$u_d=\tfrac{2}{3}c_0 \quad \text{and} \quad h_d=\tfrac{4}{9}h_0 \tag{4}$$

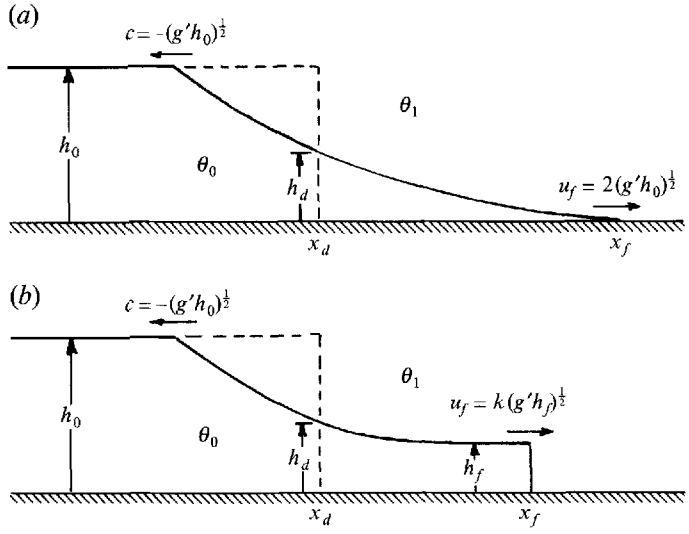

FIGURE 1. Dam-break problem using the method of characteristics. (*a*) Saint-Venant's solution. (*b*) Solution subject to a front condition as expressed in (5).

for all time. Early laboratory experiments by Schoklitsch (1917) produced good agreement with the upstream-propagating depression wave, but the propagation downstream progressed at about one half the theoretical estimate.

Abbott (1961) recognized this discrepancy and suggested that the front of the cold pool advances like a 'wall' of fluid. On dimensional grounds, he proposed that

$$u_f = k(g'h_f)^{\frac{1}{2}} \tag{5}$$

at the front of the expanding pool. For $k \geqslant 1$, this 'front condition' produces shallow-water solutions that exhibit a zone of constant state behind the leading edge, as shown in figure 1(*b*), in which

$$u_f = \frac{2kc_0}{2+k}, \quad h_f = h_0\left(\frac{2}{2+k}\right)^2 \tag{6}$$

in order to satisfy (3) and (5). In this situation, disturbances near the front cannot propagate back to the reservoir, and the critical conditions (4) at x_d maintain 'control' of the downstream-propagating gravity current.

The results characterized by (5) and (6) still leave the gravity-current propagation undetermined to a constant factor k. In fact, one can obtain solutions to (1)–(2) for k ranging over $0 \leqslant k \leqslant \infty$ (corresponding to $0 \leqslant u_f \leqslant 2c_0$), and imagine realizing these solutions by placing a piston at the leading edge of the cold pool and drawing it downstream at any constant speed u_f in this range. Thus, an additional external condition is required to determine the front condition that takes into account flow outside the cold pool. Keulegan (1950) recognized that Saint Venant's solution (see figure 1*a*) is altered by surface resistance. However, this interpretation does not suggest a means for deducing k.

Abbott argued that 'stability considerations' would require $k = 1$ and thus the constant zone would extend all the way back to the dam site x_d. Fannelop & Waldman (1972) also proposed that $k = 1$ at large times based on reasoning that the flow at the leading edge of a gravity current is similar to a hydraulic jump. However, the nose of a gravity current cannot be viewed as such since no fluid passes through the front. The

ambiguity of arguments such as these left the investigations of gravity-current propagation based on hydraulic theory without a clear resolution.

2.2. *Steady-state analyses*

In the atmosphere, the initial conditions that produce gravity currents are generally either not well understood or too complex to be described in a generalized analysis. Recognizing that gravity currents often exhibit a nearly constant shape and speed, other investigators followed an independent line of inquiry, assuming that the gravity current achieves a steady-state structure, and evaluating its properties without regard to the specific conditions that produced it.

Based on a steady-state inviscid model, von Kármán (1940) derived an expression for gravity-current propagation in an infinitely deep medium. In a coordinate framework moving with the nose of the gravity current, a flow with a constant speed $-U$ approaches from the right, as indicated in figure 2(*a*). He assumed that the fluid within the cold pool is stagnant and that the height H far behind the heads tends to a constant and $u_l = -U$. Applying the inviscid Bernoulli equation along the fluid interface between the stagnation point having pressure p_s and a location l far behind the head, and using the hydrostatic equation at l, von Kármán obtained

$$p_l(H)+\tfrac{1}{2}U^2 = p_s = p_l(0) = p_l(H)+g'H$$

or

$$U = (2g'H)^{\frac{1}{2}}, \tag{7}$$

which has been widely quoted in the literature.

In a more comprehensive analysis, Benjamin (1968) developed solutions for steady gravity currents in a finite-depth channel (see figure 2*b*) in which dissipation could occur. To summarize Benjamin's analysis, we employ the shallow anelastic equations of motion, which contain the essential physics of the problem. For steady flow, the horizontal momentum equation is simply

$$\frac{\partial u^2}{\partial x}+\frac{\partial uw}{\partial z}+\frac{\partial p}{\partial x} = \frac{\partial \tau_{xx}}{\partial x}+\frac{\partial \tau_{xz}}{\partial z}, \tag{8}$$

where (u, w) are velocity components in the (x, z) coordinates, p is a modified perturbation pressure, and τ represents either the viscous or turbulent shear stress. Far from the leading edge of the cold pool, the vertical momentum equation reduces to the hydrostatic relation

$$\frac{\partial p}{\partial z} = g\frac{\theta-\theta_1}{\theta_1}. \tag{9}$$

Integrating (8) from a point r far ahead of the leading edge (to the right in figure 2) to a point l far behind and across the channel of width d, the stress terms vanish (assuming zero-stress wall conditions and that turbulent fluctuations are weak far downstream), producing the flow-force balance

$$\int_0^d (p_r+U^2)\,\mathrm{d}z = \int_0^d (p_l+u_l^2)\,\mathrm{d}z. \tag{10}$$

Assuming $p_r = 0$ far ahead, $p_s = \frac{1}{2}U^2$ at the stagnation point x_s. Far behind the head, applying (9) yields $p_l = \frac{1}{2}U^2-g'z$ within the cold pool with $p_l(H) = p_l(d) = \frac{1}{2}U^2-g'H$ above, and continuity requires $u_l = -Ud/(d-H)$. Substituting these relations into (10) defines the velocity required to maintain a steady flow, and yield Benjamin's well-known formula

$$\frac{U}{(g'H)^{\frac{1}{2}}} = \left(\frac{2(1-\alpha)(1-0.5\alpha)}{1+\alpha}\right)^{\frac{1}{2}}, \tag{11}$$

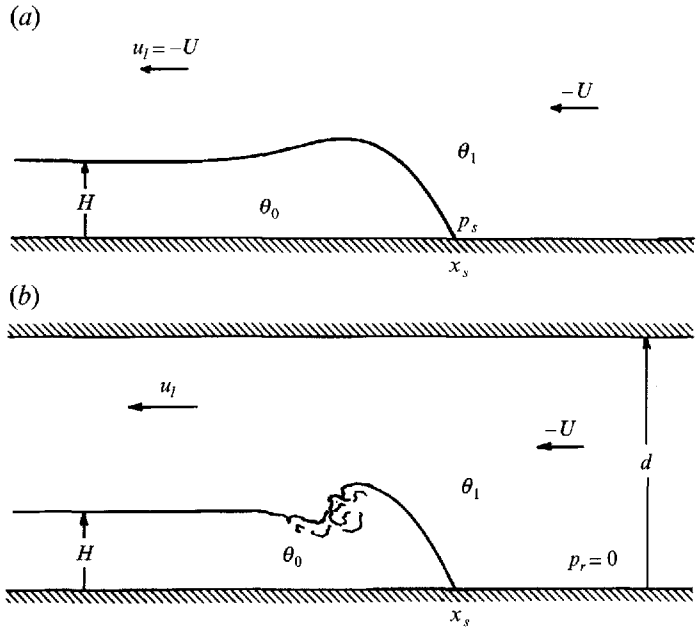

FIGURE 2. (*a*) Steady inviscid gravity current proposed by von Kármán. (*b*) Steady gravity current in channel analysed by Benjamin.

where $\alpha = H/d$. The factors involving α represent the 'finite-depth' effect and cause the gravity current to propagate more slowly as the channel depth decreases.

A steady propagating cold pool is analogous in many respects to steady flow past a semi-infinite half body. The drag D on the cold-pool half-body must just balance the net horizontal pressure (motive) force within the cold pool, such that

$$D = \int_0^H \{p_l(z) - p_l(H)\}\,\mathrm{d}z = \tfrac{1}{2}g'H^2. \tag{12}$$

For inviscid flow past a half-body, the drag must vanish as $d \to \infty$ (cf. Prandtl & Tietjens 1934, p. 118), and, therefore, this motive force cannot be balanced. Thus, Benjamin argued that von Kármán's steady-state energy-conserving flow cannot exist. This contradiction is apparent in the above flow-force balance; using the inviscid pressure $p_l = \frac{1}{2}(U^2 - u_l^2)$ instead of $p_l = \frac{1}{2}U^2 - g'H$ (which are asymptotically identical as $d \to \infty$), (10) yields

$$\frac{U}{(g'H)^{\frac{1}{2}}} = \frac{1-\alpha}{\alpha^{\frac{1}{2}}} \to \infty \quad \text{as} \quad \alpha \to 0. \tag{13}$$

Although (11) reduces to von Kármán's result (7) as $\alpha \to 0$, Benjamin argued that this is 'no more than a coincidence'.

To account for energy dissipation, Benjamin introduced a head loss Δ along each streamline that is constant with height. Thus, $g'\Delta = -p_l + \frac{1}{2}(U^2 - u_l^2)$ requires that

$$\frac{\Delta}{H} = \frac{\alpha(1-2\alpha)}{2(1-\alpha^2)}, \tag{14}$$

corresponding to an overall dissipation rate $e_d = \rho U\, dg'\Delta$. Although $\Delta \to 0$ as $\alpha \to 0$, it cannot be neglected in p_l since in this limit, the integral of $g'\Delta$ across the channel is

exactly the drag expressed in (12). Consequently, the inviscid assumption ($\Delta = 0$) is valid only for $\alpha = \frac{1}{2}$.

Benjamin's assumption that the head loss along streamlines passing over the gravity current is independent of height is admittedly unrealistic. In observed gravity currents, the dissipation is concentrated in the vicinity of the interface between the two streams, and flow in the upper portion of the channel may remain inviscid far downstream. (This result is confirmed in our numerical simulations in §4.) To evaluate the sensitivity of Benjamin's result to this assumption, we have derived an alternative expression for the propagation speed and dissipation assuming that the head loss is localized in the vicinity of the cold pool. The details of this derivation are presented in the Appendix. This analysis yields results that are nearly indistinguishable from those derived by Benjamin, providing further support for the robust nature of his result. The insensitivity of the gravity-current propagation to the distribution of the dissipation suggests that (subject to verification in §4) numerical simulations of gravity currents may not depend strongly on the details of the parameterized turbulent mixing. Rather, the turbulent diffusion may act to produce an overall dissipation that just balances the motive force of the cold pool.

2.3. *Combined initial-value and steady-state theory*

A logical reconciliation of the initial-value and steady-state approaches described above is achieved by solving the time-dependent hydraulic equations together with a front condition obtained from a steady-state flow-force balance across the leading edge of the gravity current. In this manner, Benjamin's formula (11) replaces (5) as the appropriate front condition. Rottman & Simpson (1983) followed an approach similar to this in solving the time-dependent two-layer shallow-water equations to investigate the propagation of relatively dense fluid from a reservoir into a channel. For the front condition at the leading edge of the advancing cold pool, they specified a modified form of Benjamin's formula:

$$\frac{u_f}{(g'h_f)^{\frac{1}{2}}} = k'\left(\frac{(1-\alpha)(1-0.5\alpha)}{(1+\alpha)}\right)^{\frac{1}{2}}, \tag{15}$$

which includes an adjustable parameter k' and becomes identical to (11) for $k' = \sqrt{2}$. Rottman and Simpson obtained solutions to the shallow-water equations for reservoir depths in the range $0 \leqslant h_0/d \leqslant \frac{1}{2}$, and through comparisons with companion laboratory experiments, found that $k' \approx 1$ provided the best agreement with their data.

2.4. *Comparisons with observed gravity currents*

The ultimate test of the validity of these theoretical formulae lies in their ability to describe the propagation of real gravity currents. A number of researchers have analysed the characteristics of observed atmospheric gravity currents and compared their propagation with idealized models (cf. Simpson 1969; Charba 1974; Wakimoto 1982; Carbone 1982; Hobbs & Persson 1982; Shapiro *et al.* 1985; Nielsen & Neilley 1990). These studies have applied front conditions of the form (5) and have obtained values of k that vary widely, ranging from about 0.7–0.8 (Simpson 1969; Wakimoto 1982) to about 1.4 (Carbone 1982). (See also Droegemeier & Wilhelmson 1987 for a tabulation of estimates for k based on atmospheric observations.) This range falls generally below von Kármán's (1940) and Benjamin's (1968) theoretical value of $\sqrt{2}$. However, in these studies, considerable uncertainty arises in estimating the depth, negative buoyancy, and propagation speed of the gravity current in a manner that is appropriate for comparison with simple theory. For example, the low values of k

reported by Simpson (1969) and Wakimoto (1982) are based on the height of the head of the gravity current which is generally much greater than the height further behind the leading edge. Furthermore, possible effects of finite channel depths have been largely ignored for atmospheric gravity currents. An exception to this is the study by Nielson & Neilley (1990) of coastal fronts in which they estimate an effective channel height as the depth of the neutrally stable layer beneath a strong temperature inversion. Analysing four different cases, they consistently found $k \approx 1.1$ associated with values of $\alpha = H/d \approx 0.2$, which is in close agreement with Benjamin's equation (11).

We also seek guidance from laboratory gravity currents since they can be produced under much more controlled circumstances. However, numerous ambiguities also arise in interpreting the relations between laboratory gravity currents and theory. Keulegan (1958) evaluated (5) for the intrusion of salt water into a fresh-water channel (lock exchange) and obtained average values of k ranging from 0.76 to 1.11 that have been referenced widely in the literature. The lower estimate is based on a current depth defined by the height of the head immediately behind the nose of the denser fluid, while the higher value results from using the height just behind the head. (The two heights differ by about a factor of two.) These estimates also depended on the effective Reynolds number for the experiment. However, Benjamin (1968) pointed out that for the highest Reynolds-number experiments, his theoretical estimate (11) for the front speed in the finite-depth channel compares well with Keulegan's experimental results. In experiments with a lock of finite width, Keulegan (1957) reported $k = 1.07$ at early time and a corresponding $\alpha = 0.21$, based on the height behind the head. This is again close to the value $k = 1.08$ obtained from (11).

Using both a modified lock-exchange experiment and one in which the gravity current is held stationary in an opposing stream, Simpson & Britter (1979) obtained propagation speeds about 20% below values predicted by Benjamin's formula for moderate values of α (0.2–0.3). However, for small α, their results approach those of Benjamin. They attributed the discrepancies with Benjamin to both surface friction and interfacial mixing. Simpson & Britter (1980) provided further evidence of the retarding effects of surface friction by altering the speed of a belt moving along the surface of the channel to investigate the effects of head and tail winds on gravity-current propagation. In experiments using the moving surface belt to approximate free-slip surface conditions, Britter & Simpson (1978) obtained gravity-current propagation speeds that appear to be significantly in excess of those predicted by Benjamin. These results will be discussed further in §5.

3. Two-layer shallow-water solutions

To better understand the viability of gravity-current front conditions derived from an idealized steady-state flow-force balance, we shall consider further the initial-value problem for a gravity current produced by the instantaneous release of a semi-infinite reservoir of cold fluid having depth h_0 in a channel of depth d. We turn first to the two-layer shallow-water equations and extend the solutions obtained previously by Rottman & Simpson (1983) to re-examine the utility of Benjamin's front condition. Within the shallow-water system, the gravity-current flow is highly compatible with the idealization assumed in Benjamin's derivation (i.e. hydrostatic, vertically homogeneous flow within each layer). We also seek to clarify the nature of the flow for depth ratios $\gamma = h_0/d$ larger than 0.5; the limiting case of $\gamma = 1$ corresponds to the so-called 'lock exchange' problem which has received special attention in the literature.

We consider two-layer flow in a channel with a rigid upper lid with subscripts 1 and

2 denoting the lower and upper layers, respectively. By eliminating the pressure from the momentum equations for each layer, the Boussinesq shallow-water equations can be expressed in the form

$$\frac{\partial u_i}{\partial t}+\frac{\partial}{\partial x}\left\{\left(\frac{1}{2}-\frac{h_i}{d}\right)u_i^2-\frac{h_j}{d}u_j^2-\frac{g'h_j^2}{2d}\right\}=0, \tag{16}$$

$$\frac{\partial h_i}{\partial t}+\frac{\partial u_i h_i}{\partial x}=0, \tag{17}$$

where (i,j) are (1, 2) and (2, 1) in equations for the lower and upper layers, respectively, and $h_1+h_2=d$. (Here, the double subscripts do not imply summation.)

For the reservoir problem, Rottman & Simpson (1983) used the additional constraint, $u_1h_1+u_2h_2=0$, to eliminate upper-layer variables from the lower-layer momentum equation, with the result

$$\frac{\partial u_1}{\partial t}+(1-2a)\frac{\partial u_1}{\partial x}+\left[1-\alpha-\frac{u_1^2}{g'd}(1-\alpha)^{-2}\right]g'\frac{\partial h_1}{\partial x}=0, \tag{18}$$

where $a=\alpha/(1-\alpha)$ and $\alpha=h_1/d$ as before. As demonstrated by Rottman & Simpson, solutions to (18) contain two modes that satisfy the characteristic equation

$$h_1\frac{\mathrm{d}u_1}{\mathrm{d}h_1}-(1-2a)u_1+c_\pm=0, \tag{19}$$

and propagate along characteristic directions with velocities (see also Schijf & Schönfeld 1953)

$$c_\pm=(1-a)u_1\pm[\alpha(1-\alpha)g'd-au_1^2]^{\frac{1}{2}}. \tag{20}$$

3.1. *Constraints on the downstream-propagating front*

In the one-layer reservoir flows discussed in §2.1, the downstream-propagating characteristic moves with a velocity $c_+=u+(g'h)^{\frac{1}{2}}$ that is always greater than the speed of the fluid u in the gravity current. Thus, for any u_f and h_f that satisfies a specified front condition, disturbances originating in the reservoir are continually overtaking the front. In the two-layer system, however, this may not always be the case, owing to the more complex propagation of characteristics exhibited in (20). Figure 3 displays the front speed U based on (11) along with the speed of the characteristic propagating toward the front c_+, obtained from (20) with $u_1=U$. As α increases, the speed of the characteristic c_+ falls below the front speed required by Benjamin's flow-force balance if the front height exceeds $\alpha=0.347$. Since the front cannot travel downstream faster than the fastest moving characteristic (otherwise cavitation would occur), the constraint

$$\alpha\leqslant 0.347 \tag{21}$$

must hold at the front for physically plausible solutions.

At $\alpha=0.347$, the front-relative flow in the upper stream passing over the front becomes just critical since the speed of the fastest downstream- (rightward in figures 1 and 2) propagating characteristic exactly coincides with the front speed. Benjamin (1966) recognized this critical state and noted that for a given channel depth, it produces the maximum front speed $(0.527(g'd)^{\frac{1}{2}})$ allowed by the flow-force balance (see figure 3) as well as a maximum in the steady-state dissipation rate (cf. figure 18). He suggested that if the receding stream is supercritical ($\alpha>0.347$), the flow might abruptly return to a subcritical $\alpha<0.347$ through a hydraulic jump. However, the

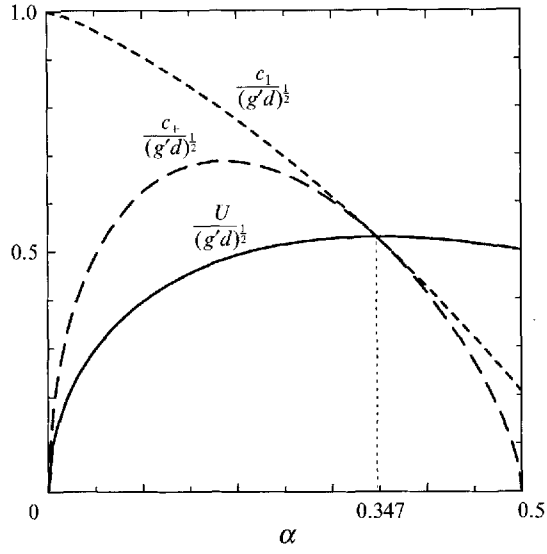

FIGURE 3. Speed of fastest-moving disturbance at the front relative to Benjamin's front speed (solid line, based on (11)) as a function of the front height $\alpha = H/d$. The long-dashed line depicts the speed of the characteristic c_+ at the front in a two-fluid system (computed from (20) with $u_1 = U$), while the short-dashed line reflects the corresponding characteristic speed c_1 for the cavity-flow problem (from (28), recognizing $\alpha' = \alpha$ and $g' = g$).

propensity for the flow to return to a subcritical state is contingent on conditions being subcritical far behind the front, and this may or may not be the case, depending on the particular gravity-current flow. For the reservoir problem, we believe the significant constraint is that limitations on the speed of the fastest-moving disturbances preclude the possibility of reaching a supercritical state at the front. This result illustrates how the propagation of gravity currents may be constrained by factors that cannot be determined solely from steady-state analyses.

Writing the steady-state form of (16)–(17) in terms of the x-derivatives of the four dependent variables, Stommell & Farmer (1952) demonstrated that for steady-state solutions to exist, either the local Froude number for the two-layer system must be unity:

$$\frac{\tilde{u}_1^2}{g'h_1} + \frac{\tilde{u}_2^2}{g'h_2} = 1, \tag{22}$$

or the flow must have no variation in x. Here, the tildes denote velocities relative to the framework in which the flow is steady. Consequently, when the front-relative flow far behind the front is subcritical, a zone of constant state forms behind the front (actually behind the non-hydrostatic breaking head), and α remains less than 0.347. However, if the flow far behind the front is supercritical relative to the front, the height and speed of the front remains steady with $\alpha = 0.347$, but the height of the fluid interface will increase with distance behind the front, forming a rarefaction wave whose slope continually decreases with time

3.2. *Constraints on the upstream-propagating front*

Upon release of the dam, a depression wave propagates back into the reservoir (upstream relative to the evolving gravity current) whose character depends on the depth ratio γ. To clarify this behaviour, consider the propagation characteristics near

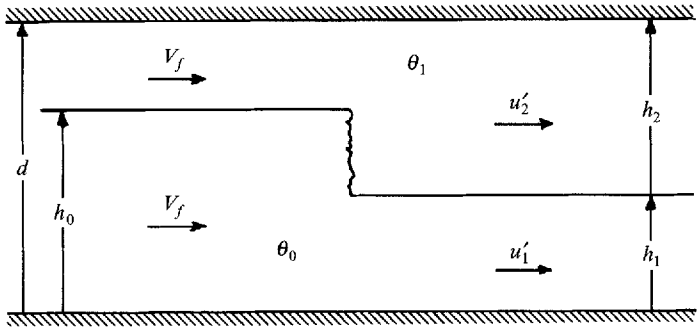

FIGURE 4. Upstream-propagating jump for the two-layer reservoir problem in a coordinate system moving to the left with the jump.

the leading edge where h_1 is close to h_0 and, therefore, u_1 is small. In this region, the speed of the upstream-propagating mode in (20) becomes

$$c_- \approx -[\alpha(1-\alpha)g'd]^{\frac{1}{2}}, \tag{23}$$

with the result that

$$\left.\frac{\partial c_-}{\partial h_1}\right|_{h_1 \to h_0} = 0 \quad \text{at} \quad \gamma = \tfrac{1}{2}. \tag{24}$$

For $\gamma < 0.5$, the leading edge of the wave travels faster (more negative) than the trailing portions and the slope of the interface will continue to decrease with time. Applying (22) in a coordinate framework moving with the leading edge, and using (23), we see that flow ahead of the wave remains just critical over this range of depth ratios. However, for $\gamma > 0.5$, as the depression wave begins to move upstream, trailing portions of the wave (having $h_1 < h_0$) propagate faster than the leading edge, and thus the front of the wave continues to steepen until it forms a discontinuity. The leading edge moves faster than the speed expressed in (23) and the flow ahead becomes supercritical. This front is a hydraulic jump according to long-wave theory, but differs from the classical jump in that it does not steepen into an abrupt discontinuity (cf. Yih & Guha 1955, and simulations in §4). Rather, the slope remains finite through the influence of non-hydrostatic effects that are outside the scope of long-wave theory.

To quantify the behaviour of the upstream-propagating jump, we examine the balances required for steady flow in a coordinate framework moving to the left with the speed of the jump V_f, as illustrated in figure 4. This analysis necessarily contains ambiguity with regard to the overall dissipation in the flow since the downstream conditions are not known. (A similar indeterminacy would occur in Benjamin's flow-force balance if dissipation was allowed within the cold fluid, in which case the surface pressure far behind the head would no longer equal the stagnation pressure.) Specifying the pressure at the top of the channel in the approaching flow to be zero, the pressure far downstream becomes

$$p_r(d) = \tfrac{1}{2}(V_f^2 - u_2'^2) + g'\Delta. \tag{25}$$

Applying the flow-force balance (10) far upstream and downstream, and using (25) and the continuity relations in the two streams, we obtain the expression

$$\frac{V_f^2}{g'd} = \frac{\gamma^2 - \alpha^2 - 2\Delta'}{[(2\gamma^2-\alpha)/\alpha] + (1-\gamma)^2(1-2\alpha)/(1-\alpha)^2}, \tag{26}$$

where $\Delta' = \Delta/d$.

Yih & Guha (1955) recognized the ambiguity resulting from the dissipation term and proposed to close the problem by assuming that the pressure along the face of the jump

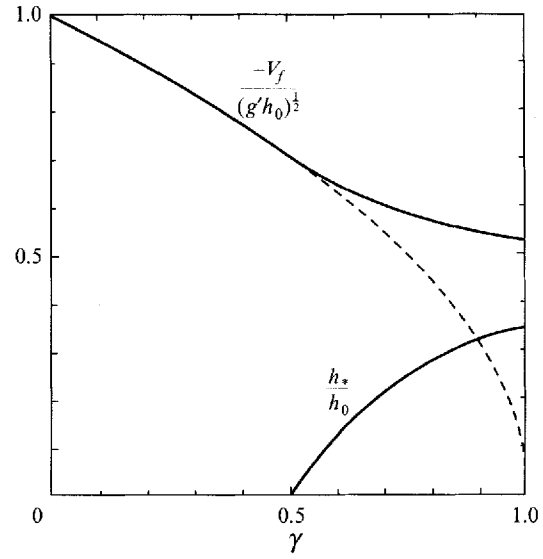

FIGURE 5. Speed (V_f) and height ($h_* = h_0 - h_1$) of the left-moving front depicted schematically in figure 4. The jump forms for $\gamma = h_0/d > 0.5$, and the dashed line represents the (critical) speed from (23) that would result if a jump did not occur.

could be approximated by the pressure in the upper fluid far downstream (to the right). Separate flow-force balances can then be written for each stream, providing an additional equation that allows Δ to be determined. If we follow this procedure, the solution as $\gamma \to 1$ yields $g'\Delta = \frac{1}{2}V_f^2$. In this limit, the front is just an inverted density current that is identical to the downstream-propagating front. However, this value of Δ together with (25) would require the surface pressure within the cold pool to be double the stagnation pressure. In fact, our two-dimensional numerical solutions (see §5) indicate that the pressure behind the head is close to the stagnation pressure. Therefore, for consistency with Benjamin's analysis (and also with the assumption of localized dissipation discussed in the Appendix), we set $\Delta = 0$. This assumption is also consistent with Armi's (1986) evaluation of weak internal hydraulic jumps.

Evaluating (26) together with (22) over the range $0.5 < \gamma \leqslant 1$, we obtain the height and speed of the left-moving jump which are displayed in figure 5. These results confirm the supercritical nature of the approaching flow for $\gamma > 0.5$ and that the height of the front reaches an upper limit $0.347d$ as $\gamma \to 1$, consistent with (22).

3.3. *Numerical shallow-water solutions*

The height and speed of the right-moving front can be computed simply by following the downstream-propagating characteristic in (19). Using the c_+ in (19) and (20), we integrate the characteristic equation in the direction of decreasing h_1, subject to the initial conditions

$$\left.\begin{aligned} u_1 = 0, \quad h_1 = h_0 \quad \text{for} \quad \gamma < \tfrac{1}{2}, \\ u_1 = \frac{-V_f h_*}{h_0 - h_*}, \quad h_1 = h_0 - h_* \quad \text{for} \quad \gamma > \tfrac{1}{2}, \end{aligned}\right\} \tag{27}$$

until Benjamin's front condition (11) is satisfied, subject to the constraint (22). V_f and h_*, shown in figure 5, represent the conditions at the left-moving jump. The behaviour of the solution derived from this procedure is depicted in figure 6. Notice that the

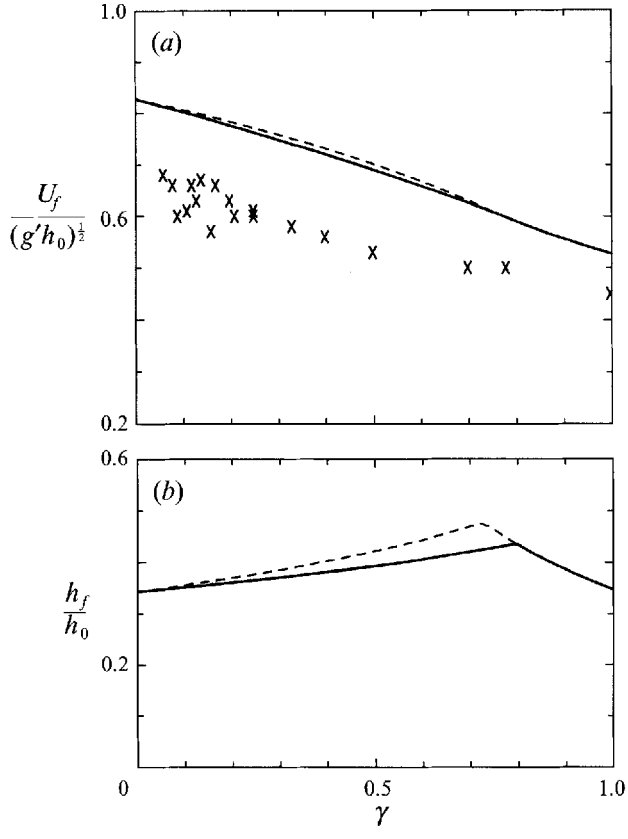

FIGURE 6. (*a*) Speed and (*b*) height of the right-moving front in the two-layer reservoir problem (solid line) as a function of the reservoir depth ratio $\gamma = h_0/d$. The dashed lines depict the respective profiles from the one-layer shallow-water equations, but using the front condition for a finite-depth channel. The points denoted by crosses reflect the results of Rottman & Simpson's (1983) laboratory experiments.

height of the front increases as γ increases until γ reaches a value of 0.79. At this reservoir-depth ratio, the criticality constraint (22) begins to limit the front height and, as γ is increased further, $\alpha = h_f/d$ remains at 0.347.

Figure 6 also displays the speed and height of the front estimated by simply combining the downstream-propagating characteristic (3) for the one-layer shallow-water system with Benjamin's front condition for a finite-depth channel, and including the criticality constraint (22). This approximation yields a good estimate of the front speed across the entire range of channel depths, but as γ increases, the front height grows noticeably more rapidly than the two-layer result, and the criticality constraint becomes active at $\gamma = 0.72$.

The two-layer front velocity is clearly higher than the values measured by Rottman & Simpson (1983), which are also shown in figure 6. By altering the front condition to (15), they found that setting $k' = 1$ provided a good fit to their laboratory data. However, this result leaves open the question of whether Benjamin's front condition is, in fact deficient or whether other simplifications in the two-layer shallow-water system are responsible for the discrepancies. We will consider these issues further in discussing the two-dimensional gravity-current simulations in §4.

To evaluate the structure of the evolving shallow-water flow, we compute solutions

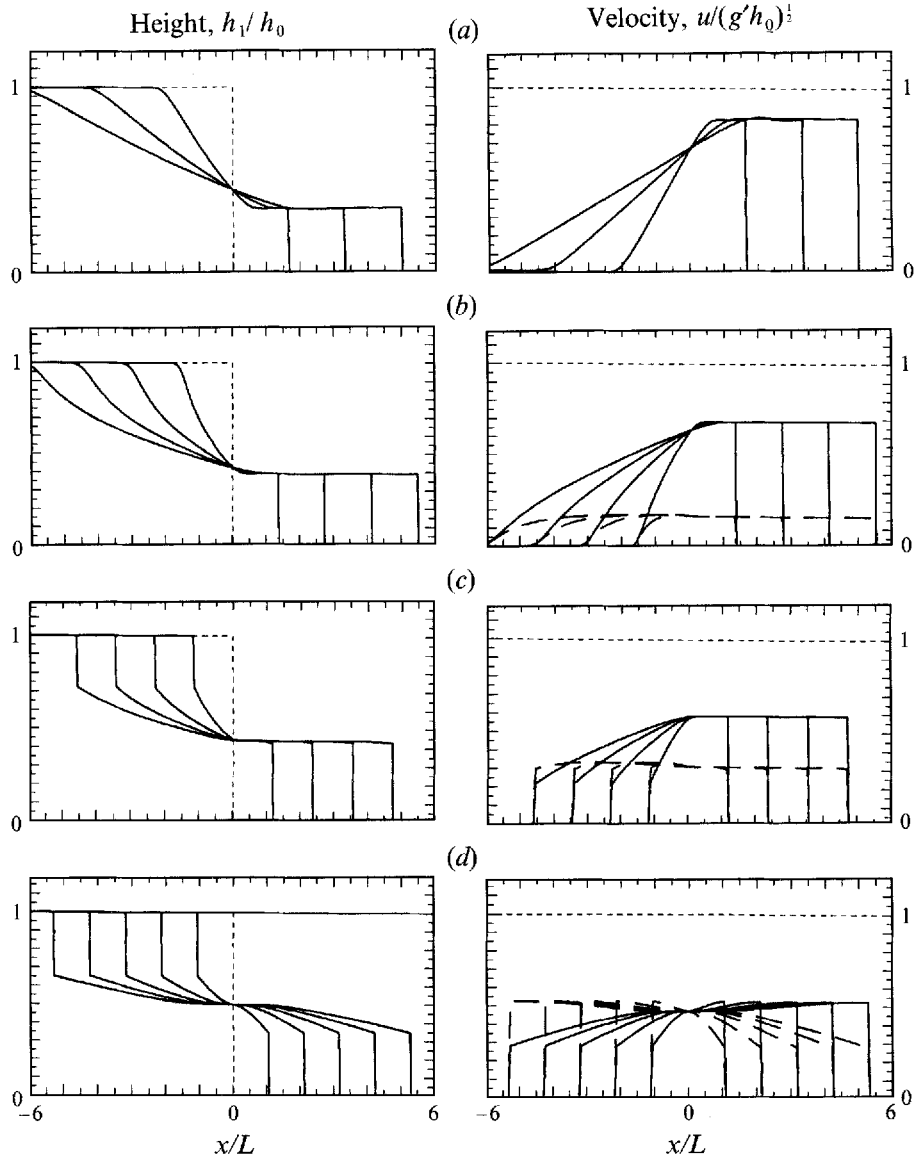

FIGURE 7. Height and velocity profiles for evolving flow in the two-layer reservoir problem in a channel for initial depth ratios $\gamma = h_0/d$ of (*a*) 0, (*b*) 0.5, (*c*) 0.8, and (*d*) 1.0. The horizontal axes are scaled using an arbitrary length L. Profiles are displayed at intervals of two dimensionless time units, with time being rendered dimensionless using $L/(g'h_0)^{\frac{1}{2}}$. The velocity plot includes both u_1 (solid lines) and $-u_2$ (dashed lines).

to (17) and (18) using a straightforward explicit leapfrog numerical scheme. We solve for u_1 and h_1 between the left- and right-moving fronts, adding grid points as the fronts progress. The boundary conditions at the left- and right-moving fronts are the same as the initial conditions (27) and the front conditions (11) and (22) used in solving the characteristic equation. The results are displayed in figure 7 for $\gamma = 0$, 0.5, 0.8, and 1. For $\gamma > 0.79$, the right-moving gravity current no longer maintains a zone of constant height behind the front. The left-moving jump that occurs for $\gamma > 0.5$ is also clearly evident.

3.4. *Character of the 'lock-exchange' problem*

In the lock-exchange problem ($\gamma = 1$), two fluids of differing density initially fill each side of a channel and propagate relative to each other after a vertical separating barrier is removed. Yih (1965), in summarizing his earlier thesis work, applied principles of overall energy conservation to fluids of slightly differing density and proposed that the depth of each fluid remains half the channel depth across the entire length between the right- and left-moving fronts. Both fronts were found to propagate at a speed $\frac{1}{2}(g/d)^{\frac{1}{2}}$, the same as Benjamin's inviscid result for $\alpha = \frac{1}{2}$.

However, this inviscid paradigm for lock-exchange flow has not been substantiated in any laboratory experiments or numerical simulations of two-fluid systems. In laboratory realizations of the lock exchange (cf. Keulegan 1957; Simpson & Britter 1979; Rottman & Simpson 1983), the flow behind the heads of both the upstream- and downstream-propagating currents exhibits substantial turbulence and the current depths (although somewhat ambiguous) are significantly less than $\frac{1}{2}d$. In fact, Simpson & Britter (1979) reported $\alpha = 0.33$ for their lock-exchange experiments and speculated that larger values might be impossible to produce experimentally. These results, together with our numerical simulations discussed in the next section, are consistent with the shallow-water solution in figure 7 for $\gamma = 1$ which, owing to the criticality constraint, maintain a depth ratio of 0.347 at the front of each current. This solution contains dissipation at the front, which is, in fact, unavoidable in two-fluid systems due to the Kelvin–Helmholtz instabilities arising in the strong shear at the interface between the two fluids.

From experiments involving the intrusion of an air cavity along the top of a water channel, both Gardner & Crow (1970) and Wilkinson (1982) concluded that the cavity depth would approach one half the channel height behind the advancing front in the limit of vanishing surface tension and that the flow would remain essentially inviscid. However, waves propagating within the fluid beneath the cavity appear to be constrained by the same criticality condition as in the two-fluid system. Since the air cavity spreads beneath the upper lid of the channel, its propagation can be compared with fronts along the lower surface in the two-layer Boussinesq system by defining velocity as positive moving in the direction of the spreading cavity and α' as the ratio of the thickness of the air cavity to the channel depth. The characteristic propagating most rapidly towards the leading edge of the cavity moves at speed $c_1 = u_1 + [gd(1-\alpha')]^{\frac{1}{2}}$, where u_1 is the velocity of the fluid beneath the cavity. At the front, continuity requires $u_1 = -\alpha' U/(1-\alpha')$ such that

$$\frac{c_1}{(gd)^{\frac{1}{2}}} = (1-\alpha)^{\frac{1}{2}} - \frac{\alpha}{1-\alpha}\frac{U}{(gd)^{\frac{1}{2}}}. \tag{28}$$

The propagation speed of the fastest-moving disturbances for the cavity problem are also displayed in figure 3 for comparison with the front speed based on Benjamin's flow-force balance (11). Although the propagation characteristics of disturbances for the cavity-flow and the Boussinesq two-fluid systems differ substantially over the range of current depths, both become critical relative to the front at the same value of $\alpha = 0.347$. Thus, based on long-wave theory, $\alpha = 0.347$ also represents the upper bound for the front height of the cavity, since heights larger than 0.347 would require the front to move faster than the fastest moving characteristic.

Interpretation of the laboratory results based on long-wave theory is complicated by the influences of viscosity, surface tension, and surface wetting, as well as the presence on non-hydrostatic effects near the leading edge. If the cavity propagation is, in fact,

controlled by this hydrostatic constraint, the front would move at the maximum speed permitted by Benjamin's flow-force balance, which is only slightly faster than the inviscid speed (0.527 *vs* 0.5), and therefore, difficult to resolve in either laboratory or numerical experiments.

4. Two-dimensional gravity current simulations

In order to gain further perspective on the validity of Benjamin's front condition as well as the accuracy of shallow-water theory in characterizing gravity-current propagation, we employ a two-dimensional numerical model to simulate atmospheric gravity currents. To maintain conditions analogous to laboratory currents, we use the following non-hydrostatic compressible Boussinesq equation set for shallow atmospheric motions:

$$u_t + uu_x + wu_z + p_x = F^u, \tag{29}$$

$$w_t + uw_x + ww_z + p_z - g\theta'/\theta_0 = F^w, \tag{30}$$

$$\theta_t + u\theta_x + w\theta_z = F^\theta, \tag{31}$$

$$p_t + c_s^2(u_x + w_z) = 0. \tag{32}$$

In these equations u and w are the horizontal and vertical velocities, θ is the potential temperature, p is the dynamic pressure, θ_0 is a reference potential temperature equal to 300 K and c_s is the sound speed having a value of 300 m s^{-1}. The subscripts (x, z, t) indicate differentiation with respect to the specified independent variable. As anticipated from Benjamin's analysis, dissipation is required in order to obtain well-behaved numerical solutions. The terms F^u, F^w, and F^θ represent turbulent mixing and numerical damping. The turbulence parameterization uses a first-order closure formulation that depends on the relative strengths of stratification and shear (Lilly 1962) and is described in Durran & Klemp (1983). A small fourth-order numerical damping term is also included to stabilize the sharp discontinuity at the leading edge of the cold pool. The general solution technique and finite differencing for the elastic system follows Klemp & Wilhelmson (1978) except that we use only second-order centred spatial differencing for these calculations.

For these simulations, we consider the same initial-value problem as in the previous section for the shallow-water equations – the instantaneous release of a semi-infinite pool of cold air (the dam-break problem). The initial cold pool is 5 km in depth with a potential temperature deficit $\Delta\theta = -10$ K. The computational domain has a horizontal dimension of 160 km and $\Delta x = \Delta z = 250$ m. A number of simulations were conducted with the channel depth varying from 5 to 50 km, thus producing results for $0.1 \leqslant h_0/d \leqslant 1.0$. In these simulations, we first consider propagation in the absence of surface friction. This is accomplished by eliminating the vertical stress divergence at the lowest grid level (one-half grid interval above the ground) rather than by requiring that vertical gradients vanish at the surface.

Solutions at $t = 15$ min are shown in figure 8 for reservoir depth ratios over the range $0.1 \leqslant \gamma \leqslant 1.0$. These gravity currents are comparable to the corresponding shallow-water solutions displayed in figure 7, with the principal differences being the non-hydrostatic circulation in the vicinity of the head. The upstream-propagating disturbances are also consistent with shallow-water theory; for $\gamma < 0.5$, a rarefaction wave develops, while for $\gamma > 0.5$, the interface steepens near the front and becomes turbulent. In this non-hydrostatic system, however, the upstream-moving front develops turbulence through shearing instability across the fluid interface (in a similar

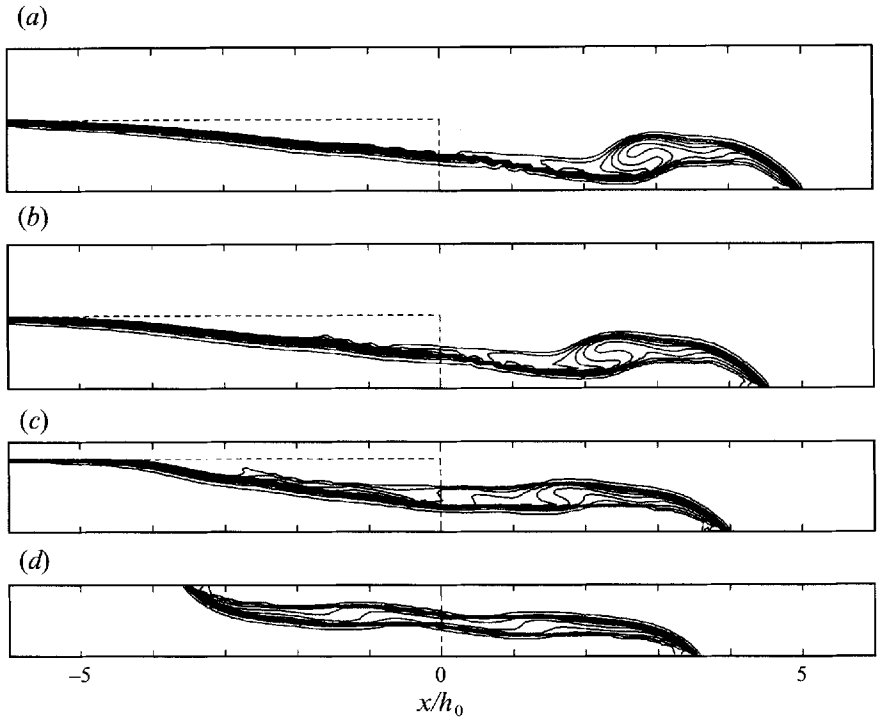

FIGURE 8. Potential temperature field at 15 min ($t(g_0'/h_0)^{\frac{1}{2}} = 7.27$) for two-dimensional simulations in a channel having an initial reservoir depth ratio $\gamma = h_0/d$ of (*a*) 0.1, (*b*) 0.5, (*c*) 0.8, and (*d*) 1.0. Contours range from 290.5 to 299.5 K in increments of one degree. Short-dashed lines denote the location of the initial reservoir.

manner to that occurring in the head of the downstream-propagating front), and does not develop the classical forward-breaking jump structure suggested by the shallow-water system.

To carry out the simulations far enough in time to produce nearly steady conditions in the region behind the head of the propagating cold pool, we found it necessary to integrate out to about 4 h. Over this time, the leading edge of the gravity current propagates a distance $x_f \sim 60h_0$–$90h_0$ downstream of the 'dam', depending on the depth ratio h_0/d. Keulegan (1958), in laboratory experiments for the lock-exchange problem, similarly found that large ratios of x_f/h_0 were required to achieve constancy in the height of the head and region immediately behind it. For computational efficiency, we translate the coordinate system at the speed of the leading edge of the cold air such that the head of the current remains nearly stationary while the reservoir translates to the left (and eventually out the left boundary). Specifying open boundary conditions along the lateral boundaries (see Klemp & Wilhelmson 1978), and making the horizontal domain large enough to contain a broad portion of the initial reservoir, the evolving flow near the head remains independent of the location of the left boundary (confirmed by comparing simulations conducted with differing domain sizes). During the entire integration period, the propagation speed of the leading edge of the cold pool remained essentially constant, and thus stationary in the translating coordinate system.

Because of the limited resolution in the model, the simulated flow in the head region does not resolve the shear layer along the interface between the two streams or the

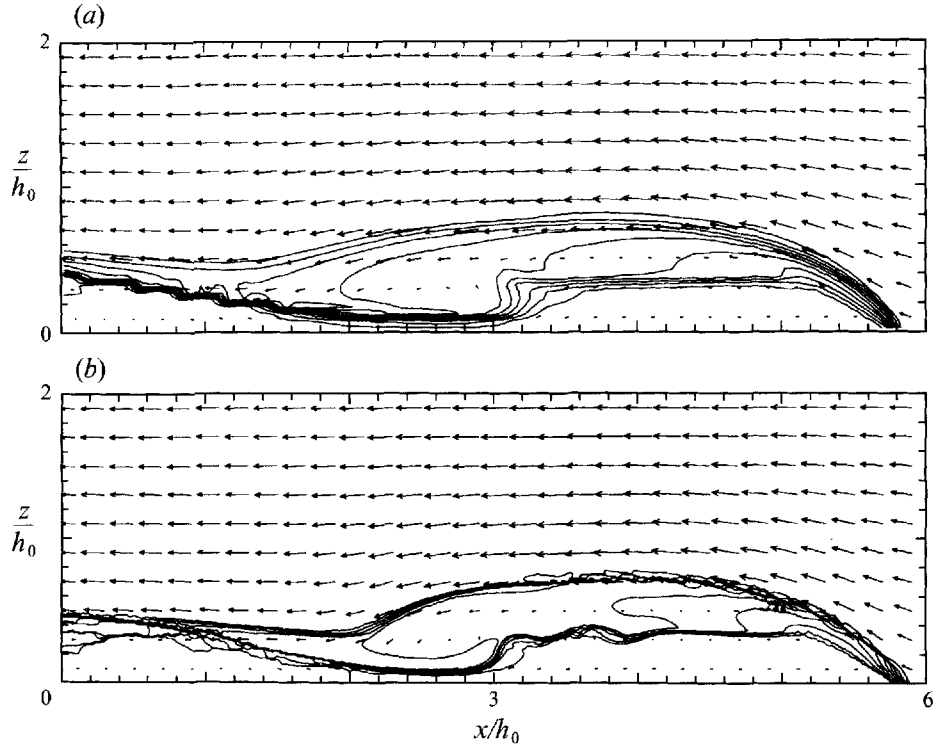

FIGURE 9. Potential temperature field (as in figure 8) at 30 min for a channel depth of $\gamma = h_0/d = 0.5$ using a spatial grid increment of (*a*) 250 m and (*b*) 50 m. Velocity vectors are scaled such that the distance between horizontal tick marks corresponds to 40 m s^{-1}. In both simulations, the coordinate system is translating to the right with respect to the reservoir at 26.0 m s^{-1}, and the actual computational domain extends to $x/h_0 = 8$.

eddies that form and disperse due to Kelvin–Helmholtz instability. However, numerous tests with varying grid sizes demonstrate that the propagation speed of the leading edge of cold air is not sensitive to resolution of the detailed structure within this mixing region. Figure 9 illustrates the comparable behaviour of simulations with respective grid sizes of 250 m and 50 m at 30 min in a channel having $\gamma = 0.5$. In spite of the factor of 5 difference in resolution (and a corresponding difference in the magnitude of the parameterized mixing), the leading edge of the cold air is in virtually the same location. This insensitivity of the propagation speed to changes in resolution and strength of mixing has also been demonstrated in other modelling studies of gravity currents (cf. Crook & Miller 1985; Droegemeier & Wilhelmson 1987). These results are consistent with our findings (see Appendix) that the propagation speed is not sensitive to the detailed distribution of head loss and that the overall dissipation adjusts to provide the required flow-force balance across the front.

Since the initial conditions in these two-dimensional gravity-current simulations are identical to those used for the shallow-water solutions described in the previous section, we may compare directly the speed of the leading edge of the cold air with the data in figure 6. These results are combined for comparison in figure 10. The front speeds in the two-dimensional simulations fall noticeably below those predicted by shallow-water theory, but are still significantly higher than those observed in Rottman & Simpson's (1983) laboratory experiments. Estimates of the thickness of the gravity current in the region behind the head (discussed further below) are plotted in figure

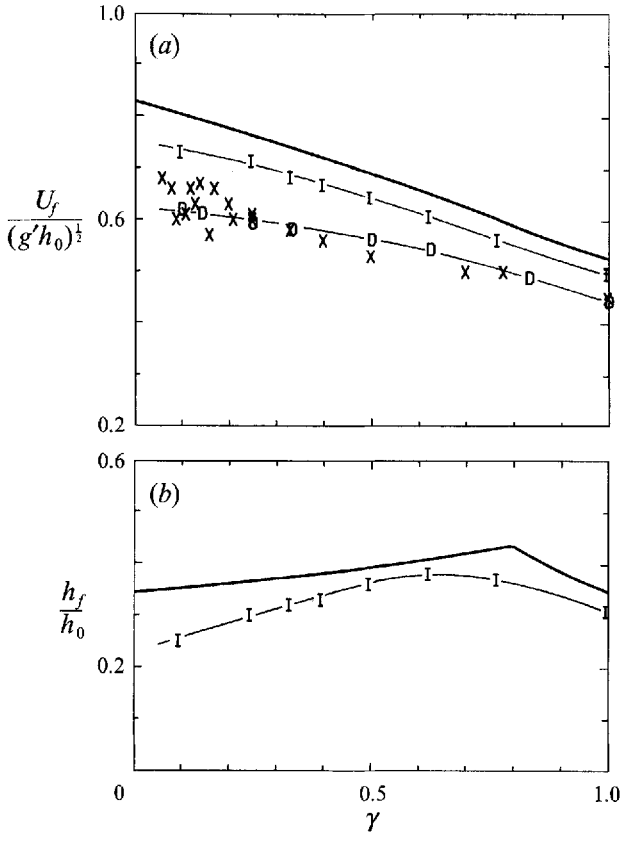

FIGURE 10. As in figure 6, but including the (*a*) speed of the gravity current and (*b*) the height behind the head obtained from two-dimensional simulations with no surface friction (displayed by the symbols I, connected by a thin solid line). Propagation speeds obtained from simulation with a surface drag coefficient of 0.005 are also included in (*a*), represented by the D symbols and connected by a thin solid line.

10(*b*) and reveal a maximum in current depth for $h_0/d \approx 0.7$ that is qualitatively similar to the behaviour in the shallow-water solutions caused by the criticality constraint (22). For the lock-exchange problem ($\gamma = 1$), the height behind the head is $h_f/d = 0.3$, which is comparable to the value of 0.347 in the shallow-water system.

We also ran simulations that included a surface drag term at the lowest grid level on the right-hand side of (29) of the form $-C_d u^2/Z$, where $Z = \frac{1}{2}\Delta z$ reflects the height of this level above the surface. Using $C_d = 0.005$ as an estimate of the drag coefficient for a turbulent boundary layer, the propagation speeds decrease to values that agree well with the laboratory data (see figure 10*a*).

In considering the overprediction of the front speed in the two-layer shallow-water system, we ask whether or not Benjamin's formula represents the correct front condition for the leading edge of the denser fluid. As mentioned in §3.3, Rottman & Simpson (1983) obtained better agreement with the laboratory experiments using $k' = 1$ in the front condition (15) instead of $k' = \sqrt{2}$ from Benjamin's formula. However, figure 10 indicates that resolving the frontal structure in a two-dimensional non-hydrostatic model with no surface friction still leaves a discrepancy with the laboratory results. At most, we would expect uncertainty in the front condition to be responsible for the difference between the top two curves in figure 10(*a*).

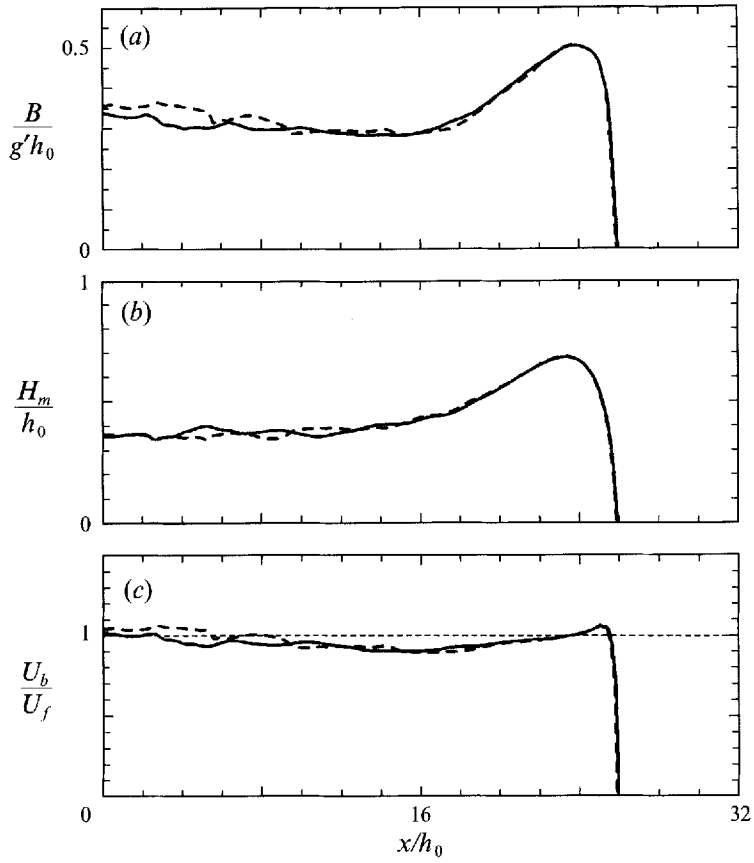

FIGURE 11. Two-dimensional simulation of the leading portion of a propagating gravity current for $\gamma = h_0/d = 0.5$. (*a*) Buoyancy integral B computed from (33), (*b*) current height H_m represented by the $\psi = 0$ streamline computed from (34), and (*c*) front speed U_b estimated from Benjamin's formula (11) at each grid column in x, normalized by the actual front speed U_f. Equation (11) is evaluated using H_m for H and B for $(g'H)^{\frac{1}{2}}$. Profiles are displayed at 3 h (dashed lines) and 4 h (solid lines).

To evaluate the validity of Benjamin's formula for these simulated gravity currents, we must estimate an appropriate depth and buoyancy deficit for the cold pool. In Benjamin's analysis, the negative buoyancy producing the net pressure increase between the surface and the top of the cold pool is just $-g'H$. We estimate this quantity from the continuously varying model fields by vertically integrating the buoyancy deficit:

$$(g'H)_m \approx B \equiv -\int_0^d \frac{g\theta'}{\theta_0}\,\mathrm{d}z. \tag{33}$$

An estimate for the depth of the gravity current can be obtained based on the height of the dividing streamline computed from the location of the $\psi = 0$ streamline in our coordinate framework in which the leading edge of the gravity current is stationary. With this approach, the top of the gravity current is defined as the height H_m at which

$$\int_0^{H_m} u\,\mathrm{d}z = 0. \tag{34}$$

The results of these calculations are illustrated in figure 11 for the case $h_0/d = 0.5$. The buoyancy integral B, computed according to (33) at each grid column in x, is

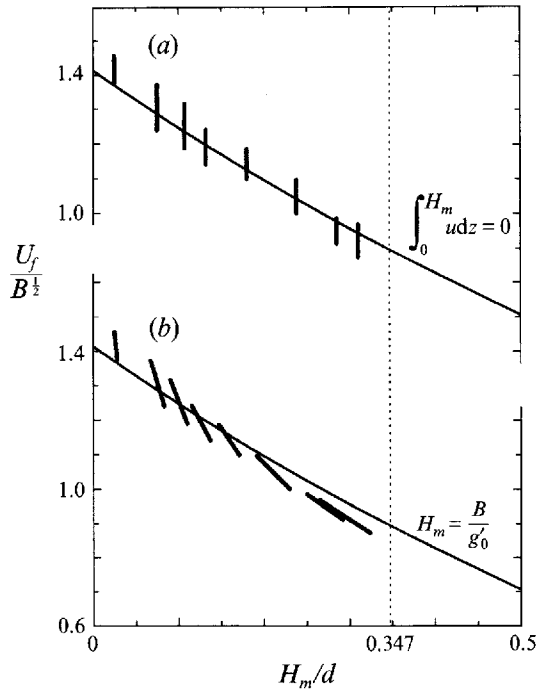

FIGURE 12. Normalized front speed in two-dimensional gravity current simulations with H_m computed from (*a*) the height of the $\psi = 0$ streamline (34) and (*b*) an effective buoyancy depth B/g_0'. Heavy bars denote the range of variation in B behind the head, while the solid curve represents Benjamin's formula (11). The dashed line indicates the critical depth ratio in the shallow-water system.

plotted at both 3 and 4 h in figure 11(*a*), and the corresponding H_m, derived from (34) are shown in figure 11(*b*).

The evaluation of Benjamin's formula requires values of B and H_m that represent the steady conditions behind the front. Inspecting figures 11(*a*) and 11(*b*), it is clear that in the region behind the head of the current, these quantities are not entirely constant over time or space. Mindful of this ambiguity, we chose an average value of B and H_m at 4 h over the interval between 1 and 3 head widths behind the head of the current as a representative estimate of the conditions behind the head. Simulations over the range $0.1 \leqslant h_0 \leqslant 1.0$, yield the results shown in figure 12(*a*). Here, the heavy bars reflect the amount of variation in B over the averaging interval in x, and are a measure of the uncertainty in the plotted data.

An alternative method of estimating H_m is to simply divide the buoyancy integral by g_0', the reduced gravity in the initial reservoir. The resulting H_m then corresponds to the effective depth of an undiluted stream having a total buoyancy deficit B. (This method was used by Crook & Miller 1985 in their analysis of two-dimensional gravity-current simulations.) Replotting the front speeds against H_m/d computed in this fashion yields the results displayed in figure 12(*b*). The heavy bars now slope with height since H_m (now proportional to B) also varies across the range in B reflected by the height of each bar.

The normalized front velocities depicted in figure 12 follow essentially along Benjamin's curve (11) and suggest that, to the level of accuracy that the comparison can be made, Benjamin's idealized flow-force balance provides a reasonably accurate characterization of the propagation of the front. Thus, we conclude that the

discrepancies between the two-dimensional and shallow-water model propagation speeds in figure 6 are not caused by Benjamin's formula (used as the front condition in the shallow-water system) overestimating the speed of the front. Rather, we believe that the lack of interfacial mixing between the two streams in the shallow-water system (clearly present in the two-dimensional simulations) is most likely responsible for the differing behaviour. Figure 10(*b*) reveals that the resulting height of the gravity current behind the head is less than the height in the shallow-water system. Through the front condition, lower heights translate into lower front speeds, as reflected in the profiles in figure 10(*a*).

In applying Benjamin's formula to observed atmospheric gravity currents, obtaining representative soundings in appropriate locations behind the head is often not possible. Figure 11(*c*) provides an indication of the sensitivity of Benjamin's estimated front speed to the position within the gravity current at which it is calculated. This is accomplished by using the pointwise values of B and H_m in figures 11(*a*) and 11(*b*) to compute a front speed U_b from (11) and (33) at each grid column in x. Beginning almost immediately behind the leading edge, the formula provides a reasonable estimate of the front speed, producing a maximum error about 10% too low in the region just behind the head.

5. Dependence on source conditions

The results discussed above indicate that Benjamin's formula may somewhat overpredict gravity current propagation speeds if the surface drag is significant. However, other studies suggest that gravity currents may propagate *faster* than predicted by Benjamin. Britter & Simpson (1978) devised laboratory experiments in a channel that approximated a free-slip lower boundary by holding a gravity current stationary with an opposing free stream in which the boundary layer was eliminated with a moving surface belt ahead of the current. Their analysis of the experimental data produced values of k' in (15) considerably in excess of $\sqrt{2}$ for small ratios of current to channel depth. (Their results probably overestimate this excess since they represented the gravity-current height based on the thickness of the region advancing toward the nose of the current rather than on the height of a mean dividing streamline, which seems more appropriate for comparison with Benjamin's analysis.) Crook & Miller (1985) obtained gravity-current speeds about 15% faster than Benjamin's estimate in numerical simulations having a fixed source of denser fluid entering the channel with a prescribed velocity, free-slip conditions at the channel walls, and an imposed mean wind to retard the movement of the gravity current across the domain. Crook & Miller concluded (correctly, we believe) that the greater-than-Benjamin speeds were caused by circulation within the cold pool in which the nose-relative surface velocity is directed toward the leading edge. This decreases the surface pressure far behind the front relative to the stagnation pressure at the nose (through Bernoulli effects) and therefore requires a stronger opposing free-stream velocity to produce the pressure difference across the current necessary to maintain a steady balance. In the two studies just mentioned, free-stream velocities were imposed to restrict the propagation of the front away from the source of the cold fluid. We believe this may be an important factor in increasing the propagation speed above values predicted by Benjamin's formula.

To illustrate a situation producing front speeds in excess of Benjamin's formula, we consider the steady-state flow-force balance for a gravity current (shown in figure 13) formed by cold fluid being pumped into a channel with velocity U_0 over a depth h_0, subject to an opposing free-stream velocity $U < 0$ just sufficient to hold the leading

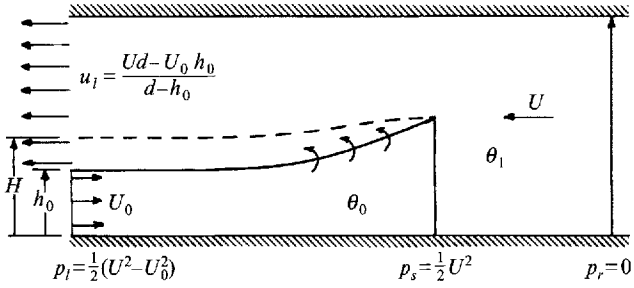

FIGURE 13. Idealization of steady-state gravity current with a constant inflow at the source and an opposing free-stream flow that maintains a stationary front relative to the source.

edge of the current stationary. Assuming a constant outflow u_l above the inflow at the left, continuity requires

$$u_l = \frac{U - \alpha U_0}{1 - \alpha}, \tag{35}$$

where $\alpha = h_0/d$. As the cold fluid approaches the stationary leading edge, it must eventually reverse direction and exit to the left above the source region. Assuming the return flow remains undiluted and exits with velocity u_l, the effective thickness of the gravity current H is given by

$$H = \frac{1+\beta}{1+\alpha\beta} h_0, \tag{36}$$

where $\beta = -U_0/U$. Here, we have purposely chosen a highly idealized flow configuration to simplify the analysis; more detailed structure, containing vertical gradients of velocity and potential temperature within the cold pool (cf. Britter & Simpson 1978; Crook & Miller 1985), can be included in a straightforward manner.

Defining the free-stream pressure as $p_r = 0$, the stagnation pressure is $p_s = \frac{1}{2}U^2$ while the surface pressure near the source becomes $p_l = \frac{1}{2}(U^2 - U_0^2)$. Applying the flow-force balance (10) across the channel yields the expression

$$\frac{U^2}{g'H} = \frac{2(1-\alpha)(1-\frac{1}{2}H/d)}{(1+\beta)[1-\beta+\alpha(1+3\beta)]}, \tag{37}$$

which has a form similar to (11), but now contains terms on the right-hand side involving U.

The normalized free-stream velocity obtained from (36) and (37) is displayed in figure 14 as a function of β. The profile for $\beta = 0$ reproduces Benjamin's result, while for small H/d, the speed increases with increasing β. For $H/d = 0$, the speeds correspond exactly to those that would be predicted by Benjamin's derivation assuming the surface pressure behind the front is $p_l = \frac{1}{2}(U^2 - U_0^2)$ instead of $\frac{1}{2}U^2$. At larger values of H/d, speeds for positive β drop below Benjamin's curve due to acceleration of the free stream as it passes over the current, which lowers the pressure in the free stream behind the front. The profiles are terminated at values of H/d where flow above the current becomes critical (estimated by $u_l^2/g'(d-H) = 1$, as discussed in §3.1).

In the above analysis, the nose-relative flow U_0 within the cold pool is an arbitrary parameter that must be specified. For the case of cold air spreading under its own weight, shallow-water solutions to the dam-break problem discussed in §2 indicate that a constant zone forms behind the front in which conditions do not depend on the

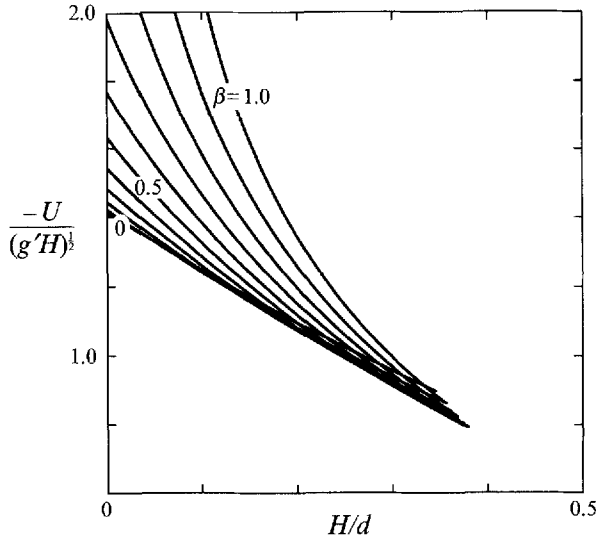

FIGURE 14. Normalized front speeds for an idealized gravity current in which the front is held stationary relative to the source, plotted as a function of $\beta = -U_0/U$ over the range $0 \leqslant \beta \leqslant 1$, in increments of 0.1.

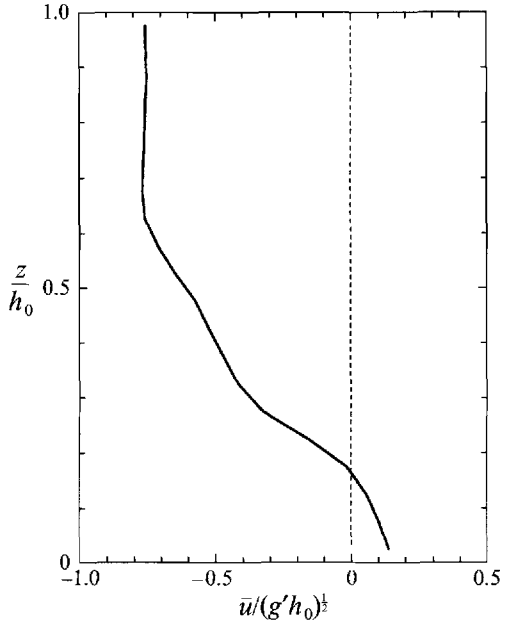

FIGURE 15. Vertical profile of horizontal velocity in region behind the head of a gravity current simulated in the two-dimensional model at 4 h for $\gamma = h_0/d = 0.1$. $\bar{u}$ represents the horizontal average of u over the interval $0 \leqslant x/h_0 \leqslant 8$ (see figure 16 for reference).

detailed evolution of the source region (reservoir). The flow speed within this constant zone is supercritical relative to the reservoir; disturbances near the front cannot propagate back to the source region and the flow near the front remains dependent only upon the downstream-propagating characteristic. However, if the flow near the front becomes subcritical relative to the source, the source region will exert a more complex influence on the front. In the one-layer shallow-water system, this occurs if

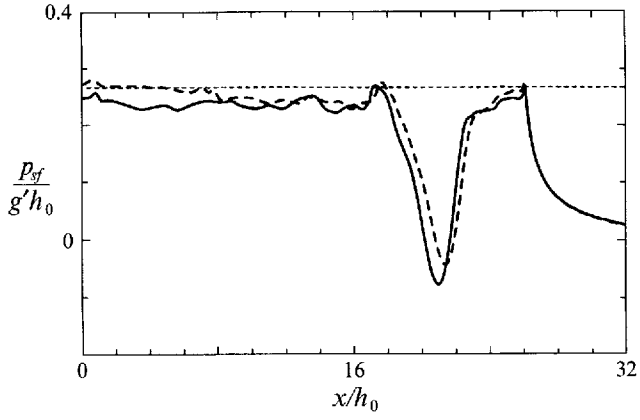

FIGURE 16. Surface pressure p_{sf} in the two-dimensional gravity current simulation for $\gamma = h_0/d = 0.1$ at 3 h (dashed line) and 4 h (solid line). The short-dashed line indicates the theoretical stagnation pressure, $\frac{1}{2}U_f^2$, at the leading edge.

front speed is restricted such that $k < 1$ in (5), in which case propagation of disturbances from the front back to the reservoir destroys the constant critical conditions (4) that provide the control for the expanding gravity current. If the reservoir is replaced by a source having a fixed U_0 over a depth h_0, a constant zone satisfying Benjamin's condition and depending only on the downstream-propagating characteristic will again form behind the front provided the front is not restricted in propagating away from the source by an opposing flow.

In the two-dimensional gravity current simulations presented in §4, the leading edge of the cold fluid is permitted to propagate freely away from the source region. In this situation, we find that the nose-relative circulation behind the front is relatively weak and has little impact on the propagation speed. Figure 15 depicts the vertical profile of horizontal velocity $\bar{u}$ in a nose-relative framework for the case $h_0/d = 0.1$ at 4 h, obtained from a horizontal average of u taken between about 2 and 3 head widths behind the leading edge. While the speed of the front relative to the undisturbed environment is 29.5 m s^{-1}, the surface velocity approaching the nose within the cold fluid is only about 6 m s^{-1}. Evaluating (37) for $\alpha \to 0$, reveals that a finite nose-relative velocity U_0 at the surface behind the gravity-current head alters the steady-state flow-force balance in a manner that increases the relative speed of the leading edge by a factor of $(1-\beta^2)^{-\frac{1}{2}}$. Thus, the circulation within the cold pool ($\beta = 0.2$) would be expected to increase the speed of the cold pool by 2%. This result is corroborated by the model surface pressure distribution, shown in figure 16, which rises to its stagnation value just behind the front, drops off sharply within the head, and then recovers to nearly the stagnation pressure in the region behind the head.

These results also appear to be consistent with results from laboratory experiments. Simpson & Britter (1979) conducted channel experiments in which β was consistently about 0.16 and obtained gravity-current speeds that did not exceed Benjamin's formula. Britter & Simpson (1978), in experiments reporting gravity-current speeds in excess of Benjamin's formula, produced values of β as large as 0.3. In Crook & Miller's (1985) numerical simulation, β was about 0.4. If the gravity current is restricted in propagating away from its source, β essentially becomes another parameter influencing the propagation, and is dependent on the strength of the source.

Based on the analogy with the shallow-water system, we expect that the circulation near the leading edge of a gravity current should become independent of the source

conditions when disturbances near the front cannot propagate back to the source region. The two-dimensional model results just described indicate that in this situation, the internal circulation is weak and does not alter the front speed significantly from Benjamin's result. We conclude, therefore, that the larger propagation speeds obtained by Britter & Simpson (1978) and Crook & Miller (1985) may arise from stronger internal circulation within the gravity current caused by an opposing flow that restricts the propagation of the front away from the source region.

6. Summary

Although there are quantitative differences between the shallow-water and the full two-dimensional systems, the shallow-water solutions reveal interesting features that appear relevant to the more complex two-dimensional simulations. In §3, we extended earlier numerical simulations of the two-dimensional shallow-water system by Rottman & Simpson (1983) to cover the entire range of reservoir depths, $0 \leqslant h_0/d \leqslant 1$, and found that constraints on both the upstream- and downstream-propagating disturbances can influence the character of the leading edge of the gravity current. If the initial reservoir has a height that is greater than one-half the channel depth, the upstream-propagating depression wave steepens into a hydraulic jump, although non-hydrostatic influences prevent it from becoming an abrupt discontinuity. Because of limitations in the speed of downstream-propagating disturbances, the front produced by the denser fluid spreading into channel is constrained such that $h_f/d \leqslant 0.347$. Thus, energy-conserving gravity currents which require $h_f/d = 0.5$ cannot be realized physically for this type of initial-value problem. This constraint may not hold for all gravity currents in a channel, since the realizability of supercritical conditions at the front may depend on how the gravity current is being generated. However, this suggests that in certain situations, knowledge of the time-dependent evolution is required to determine the long-lived or steady properties of the gravity current.

Although the two-dimensional shallow-water solutions using Benjamin's front condition leads to an overprediction of fronts speeds observed in laboratory experiments, this result does not reveal whether the discrepancy is due to inadequacies in the front condition or in other aspects of the shallow-water system. Our two-dimensional simulations with the continuous Boussinesq equations indicate that, in fact, Benjamin's (1968) analysis provides a good overall representation of the essential dynamics of a steady propagating gravity current and that his idealized flow-force balance leads to reasonable estimates for the speed of the leading edge. Comparison of the non-hydrostatic numerical simulations with the shallow-water results indicates that the overprediction of the front speed in the shallow-water system is due to the lack of interfacial mixing between the two layers and the absence of surface friction rather than deficiencies in Benjamin's front condition. Although surface friction may have significant influences on gravity-current propagation (cf. figure 10), its effects are difficult to generalize since it depends on situation-specific factors such as ground-relative propagation speed and surface roughness, and its presence may prohibit the development of steady-state characteristics in the vicinity of the front.

While freely propagating gravity currents appear to satisfy Benjamin's formula, currents retarded or held stationary relative to their source may produce front speeds relative to the free-stream flow that significantly exceed Benjamin's result owing to enhanced internal circulation within the current. In these situations, an extra parameter enters the problem and may produce behaviour that is very different from a classical gravity current. (For example, a current could be maintained in the absence

of any density differences between the two streams.) In fact, atmospheric gravity currents frequently are constrained from propagating away from their source region. A commonly occurring example is the cold-air outflow from a squall line in the presence of significant low-level wind shear (cf. Thorpe, Miller & Moncrieff 1982; Rotunno, Klemp & Weisman 1988). In these situations, the circulation within the gravity current may be fundamentally dependent on the detailed influence of the source region. If this occurs, propagation of the current depends on additional factors that cannot be known *a priori*.

In this study, we have considered only gravity currents propagating in neutrally stable environments in the absence of vertical wind shear. Clearly, both stability and wind shear are often present in the vicinity of atmospheric gravity currents and further complicate their behaviour. Stable layers can act as an effective 'channel lid' for the flow (cf. Nielson & Neilley 1990) or produce undular bores that propagate ahead of the gravity current (cf. Crook & Miller 1985). Vertical wind shear introduces another source of circulation that interacts with buoyancy-generated circulation within the gravity current. In these situations, the free-stream flow may not simply pass over the gravity current and continue downstream; rather, a significant portion of the flow may reverse direction and return upstream at upper levels (cf. Rotunno *et al.* 1988; Moncrieff & So 1989). These issues remain to be investigated in future research.

The authors wish to thank Larry Armi for numerous stimulating discussions and helpful suggestions during the course of this research.

Appendix. Flow-force balance with localized dissipation

Benjamin's (1968) derivation of the front condition for a steady gravity current assumes that flow in the free stream remains uniform far downstream as it passes over the cold pool and, therefore, that the head loss is independent of height. In real gravity currents, the dissipation is concentrated in the vicinity of the interface between the two streams, and flow in the upper portion of the channel may remain inviscid far downstream. (This result is confirmed in our numerical simulations in §4.) We present here an alternative derivation for the propagation speed and dissipation assuming the head loss is localized in the vicinity of the cold pool, and demonstrate that the resulting conditions are nearly indistinguishable from those derived by Benjamin.

We consider the steady gravity current as illustrated in figure 17, in which the free-stream flow ($u_r = U$) has velocity $u_l(z)$ far downstream, with $u_l(d) = U_l$ at the top of the channel. (For simplicity, we assume that the right-to-left flow has positive velocity.) Thus,

$$U_l = \frac{Ud+Q}{d-H}, \tag{A 1}$$

where Q is the integrated velocity deficit:

$$Q = \int_H^d (U_l - u_l)\,\mathrm{d}z. \tag{A 2}$$

Assuming that flow near the top of the channel is inviscid, the Bernoulli equation requires $p_l(d) = -\frac{1}{2}(U_l^2 - U^2)$. Integrating p_l to the surface and equating it with the stagnation pressure $p_s = \frac{1}{2}U^2$ yields

$$U_l = (2g'H)^{\frac{1}{2}}. \tag{A 3}$$

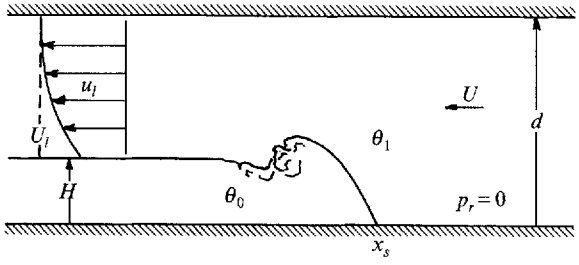

FIGURE 17. Steady gravity current in a channel with dissipation localized near the current interface.

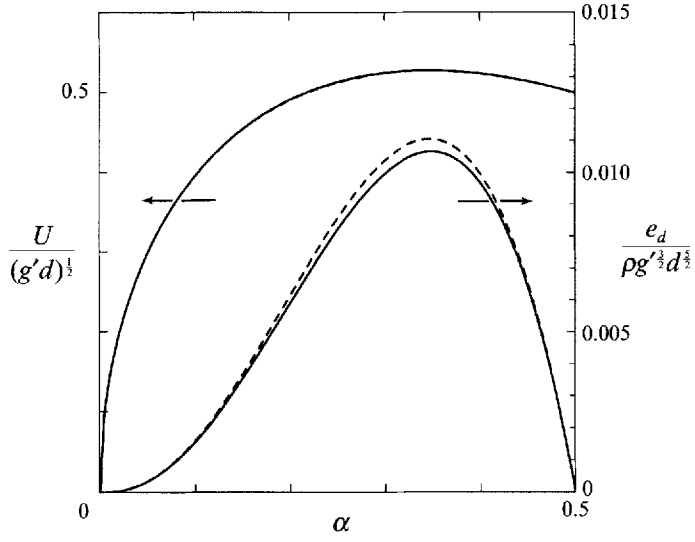

FIGURE 18. Propagation speed U and dissipation rate e_d for a steady gravity current from an analysis allowing non-uniform head loss (solid lines) and from Benjamin's analysis (dashed lines) as a function of the front height $\alpha = H/d$. Profiles are rendered dimensionless using the values from Benjamin's analysis at $\alpha = 0$.

Employing the usual wake approximation, we assume that the velocity deficit far downstream becomes small (Batchelor 1967, p. 349), such that

$$\int_H^d u_l^2 \, dz = \int_H^d [U_l^2 - 2U_l(U_l - u_l) + (U_l - u_l)^2] \, dz$$
$$\approx U_l^2(d-H) - 2U_l Q. \tag{A 4}$$

Thus, using (A 1), (A 3), and (A 4), the flow-force balance (10) reduces to

$$\frac{U}{(g'H)^{\frac{1}{2}}} = \sqrt{2}\{2-(1+2.5\alpha)^{\frac{1}{2}}\}. \tag{A 5}$$

As illustrated in figure 18, this expression is nearly identical to Benjamin's equation (11).

The dissipation rate due to the cold pool is represented by

$$e_d = \rho \int_H^d u_l g' \Delta \, dz, \tag{A 6}$$

which for Benjamin's case of uniform head loss, can be evaluated using (14). With head loss localized in the vicinity of the cold pool, this expressions becomes

$$e_d = \rho \int_H^d u_l [p_r - p_l + \tfrac{1}{2}(U^2 - u_l^2)]\, \mathrm{d}z. \tag{A 7}$$

Again neglecting terms that are second order in $U_l - u_l$, we obtain

$$e_d = \frac{\rho U^2 Q}{(1-\alpha)^2}, \tag{A 8}$$

where

$$\frac{Q}{U_l H} = \frac{(1+2.5\alpha)^{\frac{1}{2}} - 1 - \alpha}{\alpha}. \tag{A 9}$$

The integrated velocity deficit Q reaches $\frac{1}{4}UH$ for $\alpha = 0$ and vanishes as $\alpha \to 0.5$. The dimensionless dissipation (A 8), along with that predicted in Benjamin's analysis, are depicted in figure 18.

The similarity of profiles displayed in figure 18 indicates that the propagation and overall dissipation are insensitive to the detailed distribution of head loss above the cold pool.

REFERENCES

ABBOTT, M. B. 1961 On the spreading of one fluid over another, Part II: The wave front. *La Houille Blanche* **6**, 827–836.

ARMI, L. 1986 The hydraulics of two flowing layers with different densities. *J. Fluid Mech.* **163**, 27–58.

BATCHELOR, G. K. 1967 *An Introduction to Fluid Dynamics*. Cambridge University Press.

BENJAMIN, T. B. 1968 Gravity currents and related phenomena. *J. Fluid Mech.* **31**, 209–248.

BRITTER, R. E. & SIMPSON, J. E. 1978 Experiments on the dynamics of a gravity head current. *J. Fluid Mech.* **88**, 223–240.

CARBONE, R. E. 1982 A severe frontal rainband. Part I: stormwide hydrodynamic structure. *J. Atmos. Sci.* **39**, 258–279.

CHARBA, J. 1974 Application of gravity current model to analysis of squall-line gust front. *Mon. Wea. Rev.* **102**, 140–156.

CROOK, N. A. & MILLER, M. J. 1985 A numerical and analytical study of atmospheric undular bores. *Q. J. R. Met. Soc.* **111**, 225–242.

DROEGEMEIER, K. K. & WILHELMSON, R. B. 1987 Numerical simulation of thunderstorm outflow dynamics. Part I: outflow sensitivity experiments and turbulence dynamics. *J. Atmos. Sci.* **44**, 1180–1210.

DURRAN, D. R. & KLEMP, J. B. 1983 A compressible model for the simulation of moist mountain waves. *J. Atmos. Sci.* **111**, 2341–2361.

FANNELOP, T. K. & WALDMAN, G. D. 1972 Dynamics of oil slicks. *AIAA J.* **10**, 506–510.

GARDNER, G. C. & CROW, I. G. 1970 The motion of large bubbles in horizontal channels. *J. Fluid Mech.* **43**, 247–255.

HOBBS, P. V. & PERSSON, P. O. G. 1982 The mesoscale and microscale structure and organization of clouds and precipitation in midlatitude cyclones. Part V: The substructure of narrow cold-frontal rainbands. *J. Atmos. Sci.* **39**, 280–295.

HOULT, D. P. 1972 Oil sprcading on the sea. *Ann. Rev. Fluid Mech.* **4**, 341–368.

KÁRMÁN, T. VON 1940 The engineer grapples with nonlinear problems. *Bull. Am. Math. Soc.* **46**, 615–683.

KEULEGAN, G. H. 1950 Wave motion. In *Engineering Hydraulics* (ed. H. Rouse), pp. 711–768. John Wiley & Sons.

KEULEGAN, G. H. 1957 An experimental study of the motion of saline water from locks into fresh water channels. *Natl Bur. Stand. Rep.* 5168.

KEULEGAN, G. H. 1958 The motion of saline fronts in still water. *Natl Bur. Stand. Rep.* 5831.

KLEMP, J. B. & WILHELMSON, R. B. 1978 The simulation of three-dimensional convective storm dynamics. *J. Atmos. Sci.* **35**, 78–106.

LILLY, D. K. 1962 On the numerical simulation of buoyant convection. *Tellus* **14**, 148–172.

MONCRIEFF, M. W. & SO, D. W. K. 1989 A hydrodynamical theory of conservative bounded density currents. *J. Fluid Mech.* **198**, 177–197.

NIELSEN, J. W. & NEILLEY, P. P. 1990 The vertical structure of New England coastal fronts. *Mon. Wea. Rev.* **118**, 1793–1807.

PRANDTL, L. & TIETJENS, O. G. 1934 *Applied Hydro- and Aeromechanics*. Dover.

ROTTMAN, J. W. & SIMPSON, J. E. 1983 Gravity currents produced by instantaneous releases of a heavy fluid in a rectangular channel. *J. Fluid Mech.* **135**, 95–110.

ROTUNNO, R., KLEMP, J. B. & WEISMAN, M. L. 1988 A theory for strong, long-lived squall lines. *J. Atmos. Sci.* **45**, 463–485.

SCHIJF, J. B. & SCHÖNFELD, J. C. 1953 Theoretical considerations on the motion of salt and fresh water. *Proc. Minn. Intl Hydraulics Conv., University of Minnesota*, pp. 321–333.

SCHOKLITSCH, A. 1917 Über dambruchwellen. *Sitzungsber. Akad Wissenschaf.* **126**, 1489.

SHAPIRO, M. A., HAMPEL, T., ROTZOLL, D. & MOSHER, F. 1985 The frontal hydraulic head: a micro-α scale ($\sim$ 1 km) triggering mechanism for mesoconvective weather systems. *Mon. Wea. Rev.* **113**, 1166–1183.

SIMPSON, J. E. 1969 A comparison between laboratory and atmospheric density currents. *Q. J. R. Met. Soc.* **95**, 758–765.

SIMPSON, J. E. & BRITTER, R. E. 1979 The dynamics of the head of a gravity current advancing over a horizontal surface. *J. Fluid Mech.* **94**, 477–495.

SIMPSON, J. E. & BRITTER, R. E. 1980 A laboratory model of an atmospheric mesofront. *Q. J. R. Met. Soc.* **106**, 485–500.

STOKER, J. J. 1957 *Water Waves*. Interscience.

STOMMEL, H. & FARMER, H. G. 1952 Abrupt change in width in two-layer open channel flow. *J. Mar. Res.* **11**, 205–214.

THORPE, A. J., MILLER, M. J. & MONCRIEFF, M. W. 1982 Two-dimensional convection in nonconstant shear: a model of midlatitude squall lines. *Q. J. R. Met. Soc.* **108**, 739–762.

WAKIMOTO, R. M. 1982 The life cycle of thunderstorm gust fronts as viewed with Doppler radar and rawindsonde data. *Mon. Wea. Rev.* **110**, 1060–1082.

WILKINSON, D. L. 1982 Motion of air cavities in long horizontal ducts. *J. Fluid Mech.* **118**, 109–122.

YIH, C.-S. 1965 *Dynamics of Nonhomogeneous Fluids*. MacMillan.

YIH, C.-S. & GUHA, C. R. 1955 Hydraulic jump in a fluid system of two layers. *Tellus* **7**, 358–366.